



# MID-AMERICA TRANSPORTATION CENTER

Report # MATC-MS&T: 133-4

Final Report

WBS: 25-1121-0005-133-4

UNIVERSITY OF  
**Nebraska**  
Lincoln

THE UNIVERSITY  
OF IOWA

THE UNIVERSITY OF  
**KU**  
KANSAS

MISSOURI  
**S&T**

LINCOLN  
UNIVERSITY  
MISSOURI



UNIVERSITY OF  
**Nebraska**  
Omaha

University of Nebraska  
Medical Center

**KU** MEDICAL  
CENTER  
The University of Kansas

## Performance of Prestressed Bridge Girders Subjected to Vehicle Impacts

**Mohamed A. ElGawady, PhD**

Professor and Alard and Sheri Kaplan Faculty Scholar  
Department of Civil, Architectural  
& Environmental Engineering  
Missouri University of Science and Technology

**Haitham Abdel Malek, MSc**

Graduate Research Assistant

**Mohanad Abdulazeez, PhD**

Postdoctoral Research Fellow

MISSOURI  
**S&T**

2024

A Cooperative Research Project sponsored by  
U.S. Department of Transportation- Office of the Assistant  
Secretary for Research and Technology

The contents of this report reflect the views of the authors, who are responsible for the facts and the accuracy of the information presented herein. This document is disseminated in the interest of information exchange. The report is funded, partially or entirely, by a grant from the U.S. Department of Transportation's University Transportation Centers Program. However, the U.S. Government assumes no liability for the contents or use thereof.

MATC

## Performance of Prestressed Bridge Girders Subjected to Vehicle Impacts

Mohamed A. ElGawady, PhD  
Professor and Alard and Sheri Kaplan  
Faculty Scholar  
Department of Civil, Architectural &  
Environmental Engineering  
Missouri University of Science and  
Technology

Mohanad Abdulazeez, PhD  
Postdoctoral Research Fellow  
Department of Civil, Architectural &  
Environmental Engineering  
Missouri University of Science and  
Technology

Haitham Abdel Malek, MSc.  
Graduate Research Assistant  
Department of Civil, Architectural &  
Environmental Engineering  
Missouri University of Science and  
Technology

A Report on Research Sponsored by

Mid-America Transportation Center

University of Nebraska–Lincoln

August 2024

## Technical Report Documentation Page

1. Report No. 25-1121-0005-133-4	2. Government Accession No.	3. Recipient's Catalog No.	
4. Title and Subtitle Performance of prestressed bridge girders subjected to vehicle impacts		5. Report Date August 2024	
		6. Performing Organization Code	
7. Author(s) Haitham AbdelMalek; <a href="https://orcid.org/0000-0003-1161-8001">https://orcid.org/0000-0003-1161-8001</a> Mohanad Abdulazeez; <a href="https://orcid.org/0000-0003-4641-9803">https://orcid.org/0000-0003-4641-9803</a> Mohamed A. ElGawady; <a href="https://orcid.org/0000-0001-6928-9875">https://orcid.org/0000-0001-6928-9875</a>		8. Performing Organization Report No. 25-1121-0005-133-4	
9. Performing Organization Name and Address Mid-America Transportation Center Prem S. Paul Research Center at Whittier School 2200 Vine St. Lincoln, NE 68583-0851		10. Work Unit No. (TRAIS)	
		11. Contract or Grant No. 69A3551747107	
12. Sponsoring Agency Name and Address Office of the Assistant Secretary for Research and Technology 1200 New Jersey Ave., SE Washington, D.C. 20590		13. Type of Report and Period Covered Final Report	
		14. Sponsoring Agency Code MATC TRB RiP No. 91994-89	
15. Supplementary Notes			
16. Abstract This study presents a numerical modeling approach that effectively models the response of prestressed girder bridges under lateral impact loads using LS-DYNA, a finite element analysis (FEA) program. The proposed methodology was validated using experimental data from reinforced concrete beam impact tests, prestressed beam impact tests, and static testing of a full-scale bridge. Thirteen models were intensively validated using existing experimental data. These validated models were then utilized to conduct a comprehensive parametric study, examining various influential factors on the dynamic response of bridge prestressed concrete girders (BPCG) when subjected to vehicle collisions. Factors investigated included vehicle speed and mass, girder span, and girder type. Semi-trailer speed up to 144 km/h and girder spans range from 15.24 to 27.43 m were investigated. It was found that the shear failure mode was directly influenced by the girder stiffness. Also, the transformation from global shear to localized shear failure occurred when the girder span increased by a factor of 1.8. A proposed value of 1520 kN was proposed for the peak impact force resulting from the tractor semi-trailer. The findings indicate that the proposed modeling technique can be effectively used to investigate the structural response of prestressed girder bridges subjected to lateral impact loads.			
17. Key Words Bridge Girder, Prestressed, Vehicle collision, Semi-trailer, Impact force, Finite Element, LS-DYNA		18. Distribution Statement	
19. Security Classif. (of this report) Unclassified	20. Security Classif. (of this page) Unclassified	21. No. of Pages 34	22. Price

## Table of Contents

Abstract.....	vii
Chapter 1 Literature Review.....	1
Chapter 2 Finite Element Modeling.....	5
2.1 Modeling of the Prestressed Concrete .....	6
2.2 Tractor Semi-trailer.....	6
2.3 Preloading Step .....	6
2.3.1 Stress Initialization.....	8
2.3.2 Coupling.....	8
2.3.3 Contacts and Constraints.....	9
Chapter 3 Parametric Study .....	11
3.1 Static Load models.....	11
3.2 Impact Load Models .....	12
Chapter 4 Analysis of results, research report, and dissemination: .....	23
4.1 Effect of the isolated girder against the full bridge.....	23
4.2 Effect of Truck Speed .....	24
4.3 Effect of Truck Mass .....	27
Chapter 5 Conclusions .....	30
References.....	32

## List of Figures

<b>Figure 1.1</b> Collision of Chevrolet pickup with bridge pier (velocity = 110 kph (69 mph)) [2].....	2
<b>Figure 1.2</b> Kinetic energy vs impact loads normalized by the AASHTO equivalent static load [2] .....	2
<b>Figure 2.1</b> Full finite element model for Texas Transportation Institute Test 7069-13 Concrete .	7
<b>Figure 2.2</b> A Flow Chart to define the Prestressing Force using *INITIAL_STRESS_BEAM keyword.....	9
<b>Figure 3.1</b> Objectives of the Experimental Data Selected for FE Model Validation.....	11
<b>Figure 3.2</b> Static testing and FE validation (the experimental cracking pattern were reproduced after (a) Chehab et al. 2018, Girder 1-Test 1 [19] (b) Chehab et al. 2018, Girder 1-Test 3, (c) Olsen et al 1992-Girder 1 -Ultimate Load Test [20], and (d) Ludovico et al. 2005 [21], Control Girder -S1.....	13
<b>Figure 3.3</b> Static testing FE validation (the experimental curves were reproduced after (a) and (b) Chehab et al. 2018 [19], (c) Olsen et al. 1992 [20], and (d) Ludovico 2005 [21] .....	14
<b>Figure 3.4</b> Experimental and FE impact force and mid-span deflection time histories with different drop heights for beam series S1616 (a) H= 0.15m, (b) H= 0.3m, (c) H=0.6m.....	15
<b>Figure 3.5</b> Experimental and FE impact force and mid-span deflection time histories with different drop heights for beam series S1322 (a) H= 0.3m, (b) H= 0.6m, (c) H=1.2m.....	15
<b>Figure 3.6</b> Experimental and FE impact force and mid-span deflection time histories with different drop heights for beam series S2222 (a) H= 0.3m, (b) H= 0.6m, (c) H=1.2m.....	15
<b>Figure 3.7</b> ML algorithms (a) Heat map of the Pearson’s Correlation coefficient, (b) Parameter Importance .....	18
<b>Figure 3.8</b> (a) Number of bridges with the span, (b) skew angle, (c) deck width.....	19
<b>Figure 3.9</b> FE models, (a) Full bridge of Modot type II; Isolated girders wot composite deck slab, (b) Modot type 2, (c) Modot type 6, (d) NU 35 girder. ....	20
<b>Figure 3.10</b> FE 3D view (a) Full bridge, and (b) Isolated girder with composite deck (01-M2- L15.24-S80-M24.9) .....	22
<b>Figure 4.1</b> FE results (a) full bridge and Isolated girder force time history, (b) full bridge damage, and (c) isolated girder damage (01-M2-L15.24-S80-M24.9) .....	24
<b>Figure 4.2</b> (a) Impact force and displacement time histories, (b) Peak impact force with speed 26	
<b>Figure 4.3</b> The contour of plastic strain Damage modes (a) at the first impact, (b) at maximum displacement (t=30 ms).....	28
<b>Figure 4.4</b> (a) Impact force-displacement time histories and damage modes for truck mass 24.9 and 36.3 tons (b) Impact time histories details .....	29

## List of Tables

<b>Table 3.1</b> Summary of the static FE validation results and the mean error .....	14
<b>Table 3.2</b> Girder description and geometric summary .....	20
<b>Table 3.3</b> FE Study Parameters .....	21

## Disclaimer

The contents of this report reflect the views of the authors, who are responsible for the facts and the accuracy of the information presented herein. This document is disseminated in the interest of information exchange. The report is funded, partially or entirely, by a grant from the U.S. Department of Transportation's University Transportation Centers Program. However, the U.S. Government assumes no liability for the contents or use thereof.

## Abstract

This study presents a numerical modeling approach that effectively models the response of prestressed girder bridges under lateral impact loads using LS-DYNA, a finite element analysis (FEA) program. The proposed methodology was validated using experimental data from reinforced concrete beam impact tests, prestressed beam impact tests, and static testing of a full-scale bridge. Thirteen models were intensively validated using existing experimental data. These validated models were then utilized to conduct a comprehensive parametric study, examining various influential factors on the dynamic response of bridge prestressed concrete girders (BPCG) when subjected to vehicle collisions. Factors investigated included vehicle speed and mass, girder span, and girder type. Semi-trailers with speeds up to 144 km/h and girder spans ranging from 15.24 to 27.43 m were investigated. It was found that the shear failure mode was directly influenced by the girder stiffness. Also, the transformation from global shear to localized shear failure occurred when the girder span increased by a factor of 1.8. A value of 1520 kN was proposed for the peak impact force resulting from the tractor semi-trailer. The findings indicate that the proposed modeling technique can be effectively used to investigate the structural response of prestressed girder bridges subjected to lateral impact loads.

## Chapter 1 Literature Review

More than 1,000 accidents occur annually in the U.S. where a truck's height exceeds the vertical clearness of a bridge. In these instances, the truck collides with the girders of the bridge, causing damage to the girders or, in extreme cases, collapse of the whole bridge (Agrawal et al. 2018). Despite being a crucial issue for many Departments of Transportation (DOTs), experimental testing and analytical models of over-height vehicle impacts with bridge girders are scarce and urgently required. This chapter reviews research relevant to vehicle impact with bridge girders. In particular, different experimental work is presented and implemented to calibrate the models. Furthermore, the effects of loading rates on concrete and steel performance is synthesized. Different material models used to model concrete under dynamic loads are also assessed.

In a recently concluded Missouri DOT (MoDOT)-sponsored project, the PI used finite element models to determine truck impact design loads for bridge columns (Fig. 1.1). Unlike the AASHTO design approach where a constant load of 600 kips was used for columns design regardless of the truck mass or speed, the proposed equation is a function of vehicle mass and speed (Fig. 1.2).

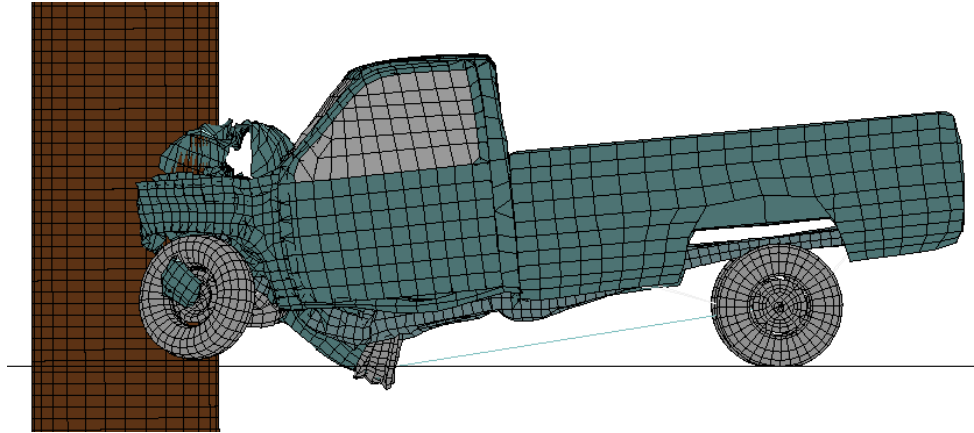


**Figure 1.1** Collision of Chevrolet pickup with bridge pier (velocity = 110 kph (69 mph)) [2]

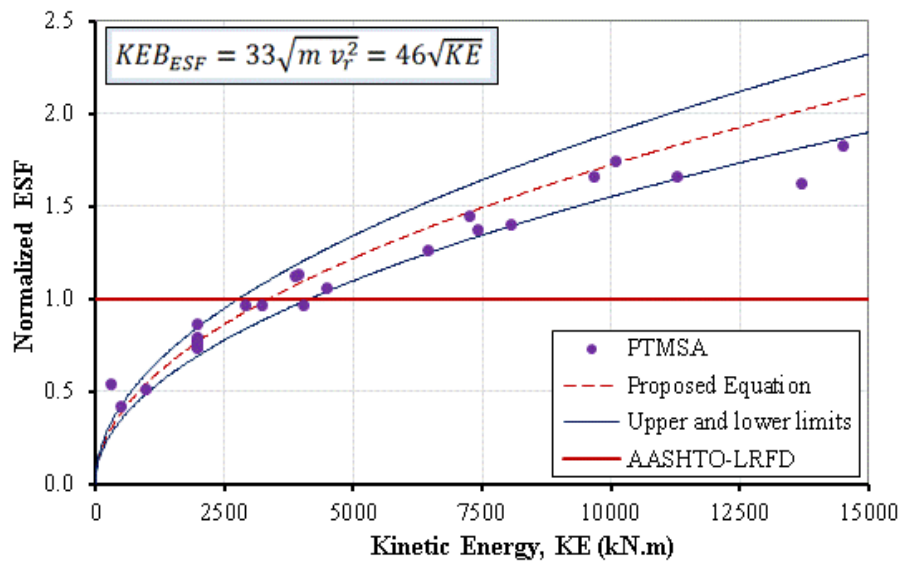


**Figure 1.2** Kinetic energy vs impact loads normalized by the AASHTO equivalent static load [2]

Agrawal et al. [1] conducted a research study that revealed 28 states out of 50 in the United States identified over-height collisions as a significant problem for their bridges. Although measures such as vertical clearance signs and warning lights have been implemented to reduce collisions, the problem still exists, and many overpasses continue to experience damage

during their service life. These over-height accidents frequently result in compromised girders, which can have serious consequences for structures' safety and performance [3-5].

Numerous drop-weight laboratory investigations have been performed on traditional reinforced concrete (RC) type members to address both flexural and shear responses [6-8]. Comparatively, only a few experimental investigations on the impact behavior of prestressed girders are available [9-10]. Finite element (FE) simulations of truck-bridge collisions have attracted a lot of interest in the research community so far. For example, Thilakarathna et al. [11] used the finite element program LS-DYNA to perform numerical simulations of axially loaded concrete columns under transverse impact. While some numerical studies [12-13] have investigated the response of bridge superstructures under impact, along with the associated failure mechanisms and collision loads, none of these studies have explored the behavior of prestressed girder bridges. The geometric nonlinearity, material nonlinearity, and contact nonlinearity, in addition to the difficulty in modeling prestressed concrete, make numerical simulation of prestressed girder bridge collisions challenging. Yet, experimental verification is limited and critically needed to establish the validity of numerical models.

The primary objective of this study is to develop a comprehensive finite element model for prestressed girder bridges and subsequently validate its accuracy through a series of rigorous procedures. Several methods for modeling prestressed concrete have been investigated using the LS-DYNA software, including stress initialization, axial beam force, and temperature-induced shrinkage. The effect of using dynamic relaxation in modeling prestressed concrete was also introduced. The selection of an appropriate concrete constitutive material model was thoroughly investigated; ensuring that the developed model appropriately represents the response of prestressed girder bridges under impact loads. Four material models were investigated and

evaluated: CSCM, CDPM, KCC, and Winfirth. A series of validation steps were carried out to ensure that the FE model accurately reflected the behavior of the real-world bridge. Once validated, a parametric study matrix was prepared to show the applicability of the FE model in capturing the response of prestressed girders under impact loads. The findings from this study are expected to contribute to the development of improved repair design strategies of prestressed girder bridges that can better withstand impact loads.

## Chapter 2 Finite Element Modeling

In the field of bridge engineering, it is of the utmost importance to understand the global behavior of large-scale bridges under impact loads. However, conducting large-scale experimental testing poses significant challenges due to the associated cost and complexity, resulting in limited available data in the literature. In addition, studying individual girders ignores the composite effects of bridges, which can have a big effect on how bridges behave as whole systems under impact loads. To overcome this limitation, a finite element (FE) model of a bridge provides a more comprehensive understanding of its global response and allow for a comparison with the response of individual girders. In this study, the commercial software LS-DYNA was used to conduct numerical simulations of prestressed girder bridges under impact loads.

A series of validation steps were carried out to ensure the FE model accurately reflected the behavior of the real-world bridge. Once validated, a parametric study matrix was prepared to show the applicability of the FE model. The library of LS-DYNA includes several material models, such as mat 001, that can be used for concrete material modeling. The different material models and their capabilities to model the dynamic response of concrete will be explored during the calibration process. The developed models will be calibrated and validated against experimental work from the literature.

The objective of this section is to provide a set of framework guidelines for effectively simulating prestressed girder bridges subject to impact loads. The finite element modeling details are presented in this section.

## 2.1 Modeling of the Prestressed Concrete

When modeling prestressed concrete in LS-DYNA, solid elements are typically used to model the concrete while beam elements are used to represent the prestressing strands. To accurately model the behavior of prestressed concrete, two essential steps are required. The first step is to set the required stress value in the prestressing strands, commonly referred to as the preloading step. This stress value is usually determined based on the design requirements and the properties of the prestressing material. In the second step, known as the coupling step, stresses are transferred from the prestressing strands to the concrete elements. This step involves the application of a transfer function that accounts for the bond between the prestressing strands and the surrounding concrete. Once the prestressing of the model is completed, the next step involves applying the transient load.

## 2.2 Tractor Semi-trailer

Over-height truck impacts commonly occur due to tractor semi-trailers in the United States. The tractor-semitrailer FE model selected for this study was extensively validated both qualitatively and quantitatively against barrier crash testing [14]. The Texas Transportation Institute Test 7069-13 model, which simulated a 1992 Freightliner FLD120 Tractor with an integral sleeper cabin, was implemented in this study (Figure 2.1). The original semi-trailer FE model has a 55-kip mass. The mass sources are the tractor, trailer, and barriers inside the trailer. The material mass density of the barrier was increased to have a total truck mass of 80 kips to increase the truck mass.

## 2.3 Preloading Step

Preloading is an important technique used in many engineering applications to improve the performance of structures under load. This technique is commonly used in LS-DYNA in the

analysis of bolted joints, where preloading is applied to the bolted connection to ensure that the joint remains tight and secure under operational loads [15-16]. LS-DYNA contains multiple preloading techniques, including temperature-induced shrinkage, interference contact force, introduced stress in solid cross-sections, and introduced force in beams. Typically, the prestressing force is gradually applied prior to conducting a transient dynamic analysis. To manage pre-force relaxation during the pseudo phase, either explicit or implicit dynamic relaxation is utilized.

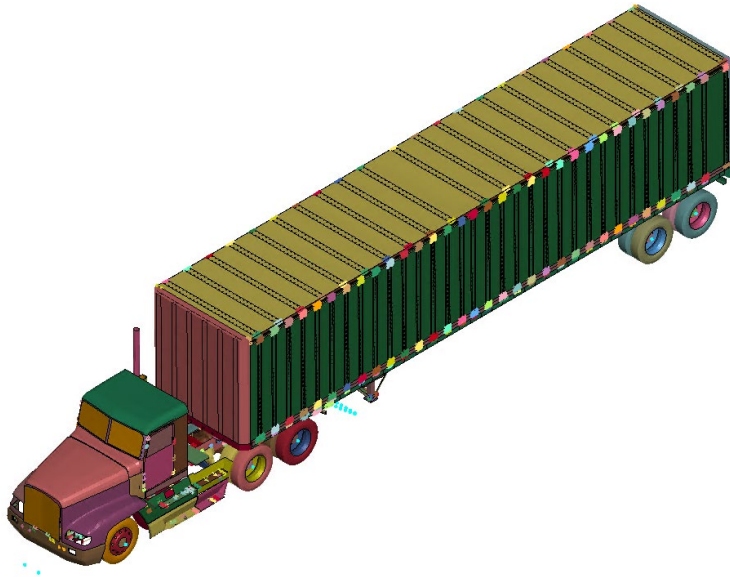


**Figure 2.1** Full finite element model for Texas Transportation Institute Test 7069-13 Concrete

In this study, three different prestressing techniques using `*INITIAL_STRESS_BEAM`, `*INITIAL_AXIAL_FORCE_BEAM`, and `*LOAD_THERMAL_CURVE` keywords were used. Each of these techniques offers unique advantages and disadvantages, and the optimal approach depends on the specific requirements of the analysis. The subsequent sections of the study will

delve into the details of each approach to provide a comprehensive understanding of their implementation within LS-DYNA.

### *2.3.1 Stress Initialization*

In LS-DYNA, the `*INITIAL_STRESS_BEAM` keyword was used to define initial stress conditions for beam elements in a finite element model. This keyword is used in the context of explicit dynamics simulations, which are commonly used in crashworthiness and impact analysis. When `*INITIAL_STRESS_BEAM` keyword is used, LS-DYNA applies an initial stress state to beam elements defined using the `*BEAM` keyword (Figure 2.2). The initial stress state can be used to simulate pre-stress conditions, such as residual stresses in a metal structure due to manufacturing processes. The initial stresses can be defined by specifying a uniform stress state, specifying a non-uniform stress state using a table of values, or using a user-defined subroutine to calculate the initial stresses. The `*INITIAL_STRESS_BEAM` keyword can be used in conjunction with other keywords in LS-DYNA, such as `*BOUNDARY_PRESCRIBED_MOTION`, `*BOUNDARY_SPC`, and `*DAMPING`, to fully define the initial and boundary conditions for beam elements in a finite element model.

### *2.3.2 Coupling*

In prestressed concrete, the selection of an appropriate coupling mechanism plays a crucial role in transferring the stresses between the strands and the surrounding concrete elements, requiring careful consideration. To accurately model the prestressing strands, tubular beam elements with the default element formulation (`ELFORM=1`), specifically Hughes-Liu beams with 2x2 Gauss quadrature, were utilized. Various coupling techniques are available in LS-DYNA, including merging reinforcing beam elements with solid concrete elements through shared nodes, using 1-D contact to tie beam elements to concrete elements and account for bond-

slip between concrete and steel, and coupling reinforcing beam elements to concrete elements using the \*CONSTRAINED\_LAGRANGE\_IN\_SOLID or CONCRETE\_BEAM\_IN\_SOLID formulation.

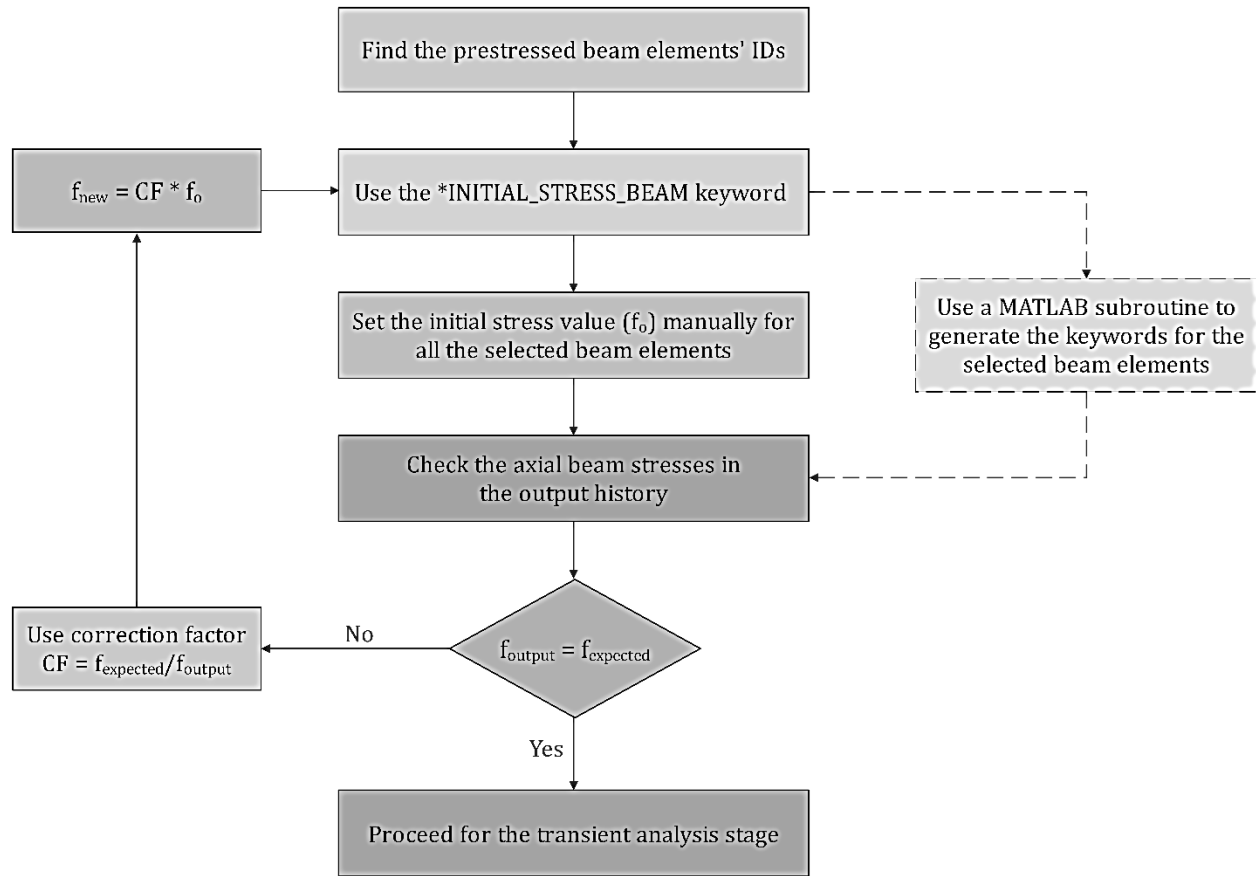


**Figure 2.2** A Flow Chart to define the Prestressing Force using \*INITIAL\_STRESS\_BEAM keyword.

### 2.3.3 Contacts and Constraints

\*AUTOMATIC\_SURFACE\_TO\_SURFACE contact was used in this study for the impact analysis. When the surface of one body penetrates the surface of another, the surface-to-surface contact algorithm is activated, and although it is fully symmetric, the designation of slave and master surfaces is arbitrary. However, it is recommended that the part with the fastest

moving speed be designated as the slave surface [17]. The penetration force ( $f_p$ ) for the slave node is computed as a function of the penetration distance in this contact algorithm.

The main output parameter of interest in impact analysis is the impact force, which is obtained during the contact process. As a result, the \*DATABASE NCFORC and DATABASE BINARY INTFOR interface force files should be integrated to record the relevant contact data. Another method for getting the impact force results is to use the \*FORCE TRANSDUCER PENALTY contact, in which the surface of the concrete segment is designated as the slave and no master is assigned.

## Chapter 3 Parametric Study

The developed FE models will be used to better understand the performance of bridge girders subjected to over-height truck impact. In particular, the effects of beam details such as initial prestressing force, number of tendons, concrete compressive strength, prestressed eccentricity, tendon characteristics, vehicle speed, vehicle type, impact angle, truck type, truck speed, and impact location will be investigated.

To validate the FE model of the bridge, three experimental data were utilized, where each serves different objectives (Fig. 3.1). The first two tests were utilized to validate the impact parameters, while the third test was employed to verify the global response of a prestressed girder bridge. Detailed information is provided in this section.

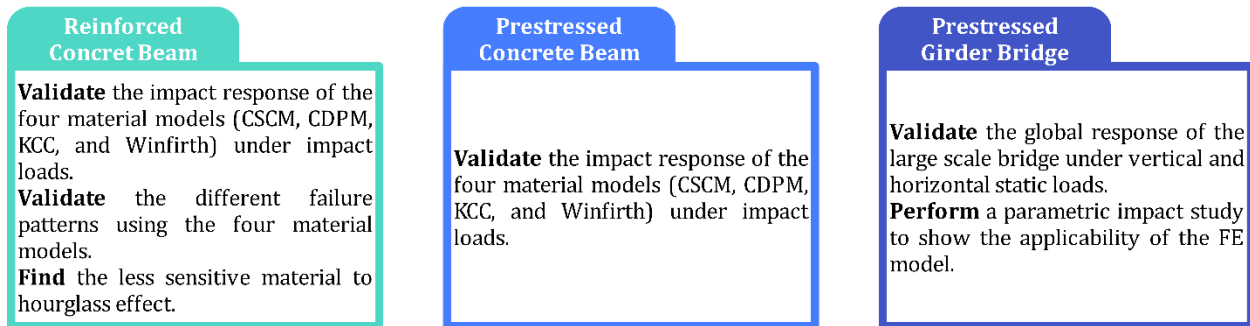


**Figure 3.1** Objectives of the Experimental Data Selected for FE Model Validation

### 3.1 Static Load models

The strand prestressing process and material models were validated for the static models under static loading. The girder concrete cracking pattern agreed considerably with the experimental test results (Fig. 3.2), and the force-deflection curves were compared both graphically as in Figure 3.3 and numerically as in Table 2. The mean absolute error of FE peak force was found to be 14%. Overall, the FE results were a good match to the test results,

indicating the prestressing process was applied successfully, and the material models could be used in further analyses.

### 3.2 Impact Load Models

The static models under impact loading were primarily validated for the contact algorithm and contact scale factors. The FE impact force and displacement time histories were examined against the test results [4, 18] (Fig. 3.4-3.6). A discrepancy between the test and FE results was noticed despite using the same FE modeling parameters. Error analyses were conducted to investigate this discrepancy further. The mean error was computed as shown in (Table 3.1). The mean was 11%, 22%, and 8% for the peak impact force, peak mid-span displacement, and impulse, respectively.

The impulse can be used as a good indicator to compare the FE against the test results, as it combines the dynamic characteristics of both the impacted beam and the impactor. In general, the FE models were in good agreement with the test results. All the FE analyses were run using LS DYNA software on a Linux cluster with four nodes of 16 CPUs and 200G memory. A 1.5-second termination time corresponds to 80 hours to complete using a Message Passing Parallel (MPP) double-precision solver.

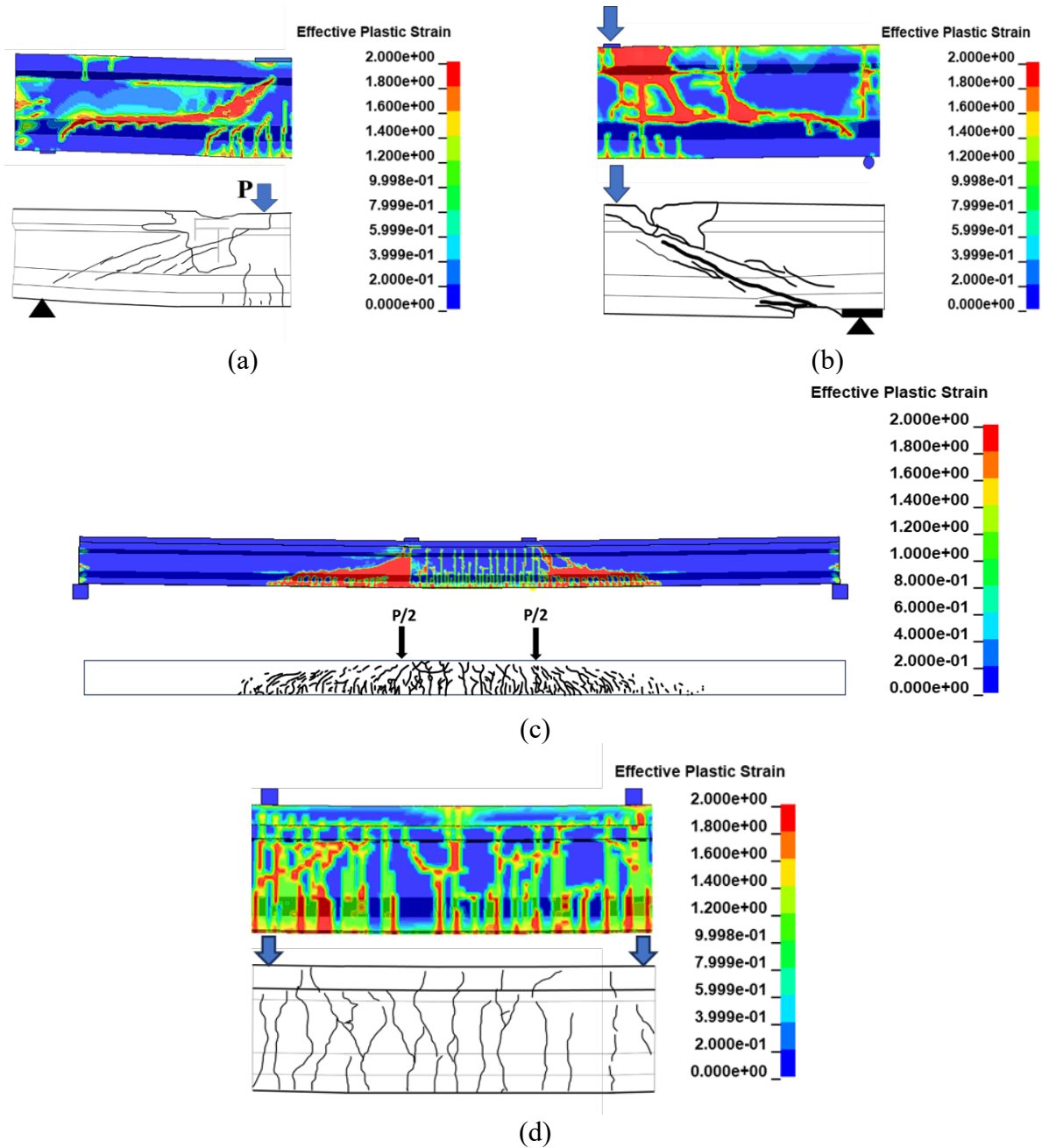


**Figure 3.2** Static testing and FE validation (the experimental cracking pattern were reproduced after (a) Chehab et al. 2018, Girder 1-Test 1 [19] (b) Chehab et al. 2018, Girder 1-Test 3, (c) Olsen et al 1992-Girder 1 -Ultimate Load Test [20], and (d) Ludovico et al. 2005 [21], Control Girder -S1

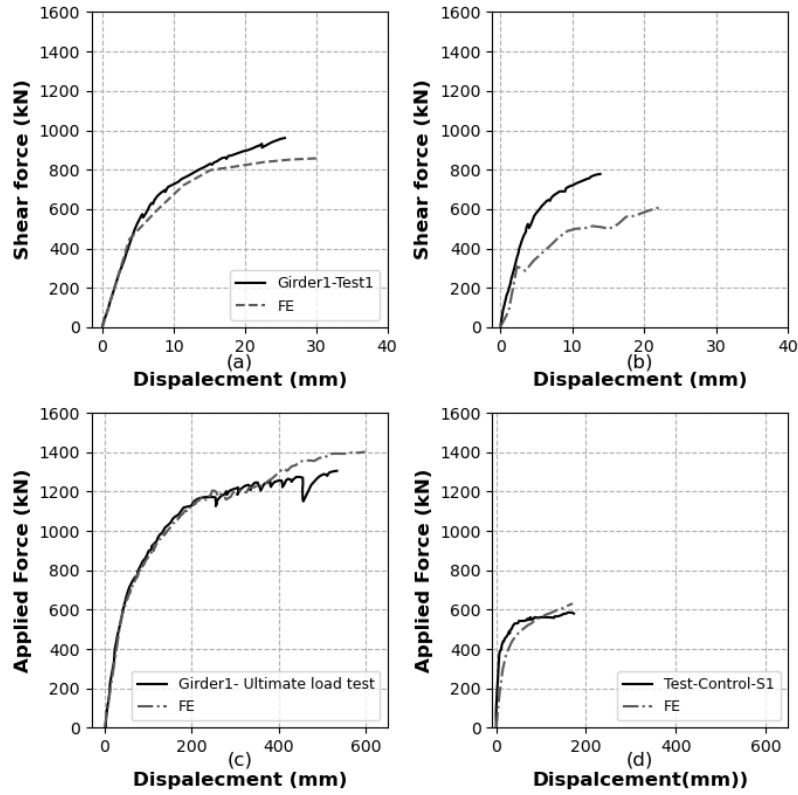


**Figure 3.3** Static testing FE validation (the experimental curves were reproduced after (a) and (b) Chehab et al. 2018 [19], (c) Olsen et al. 1992 [20], and (d) Ludovico 2005 [21])

**Table 3.1** Summary of the static FE validation results and the mean error

Model	Testing type	Test	FE	Error
		Maximum Force (kN)	Maximum Force (kN)	Maximum Force (kN)
G1-Test1(Chehab et al., 2018)	Shear	790	848	0.07
G1-Test3 (Chehab et al., 2018)	Shear	965	611	0.36
G1 (Olsen, 1992)	Flexural	1290	1400	0.08
Test-Control (Ludovico, 2005)	Flexural	595	625	0.05

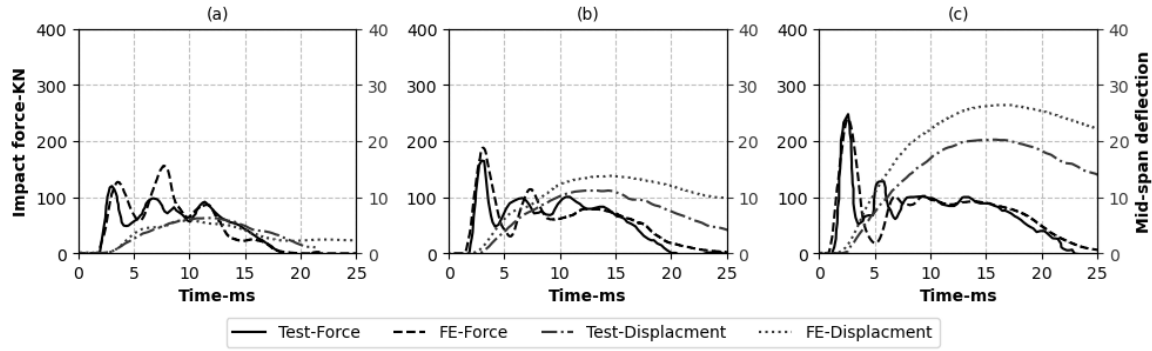


**Figure 3.4** Experimental and FE impact force and mid-span deflection time histories with different drop heights for beam series S1616 (a)  $H= 0.15\text{m}$ , (b)  $H= 0.3\text{m}$ , (c)  $H=0.6\text{m}$

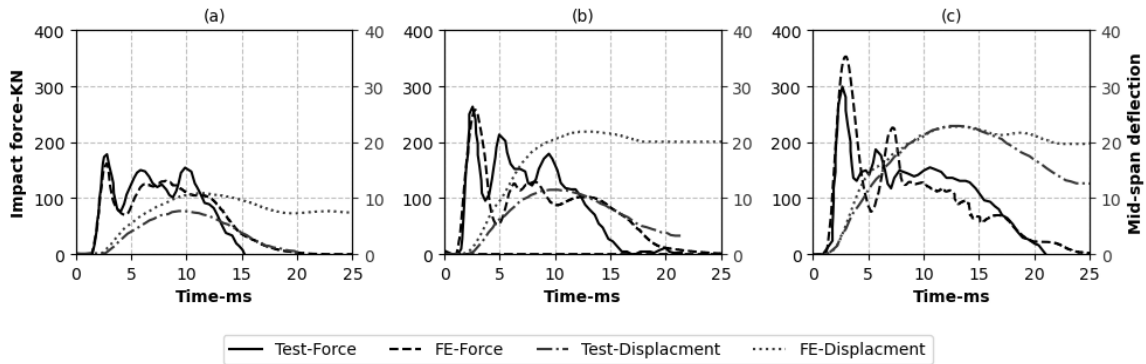


**Figure 3.5** Experimental and FE impact force and mid-span deflection time histories with different drop heights for beam series S1322 (a)  $H= 0.3\text{m}$ , (b)  $H= 0.6\text{m}$ , (c)  $H=1.2\text{m}$

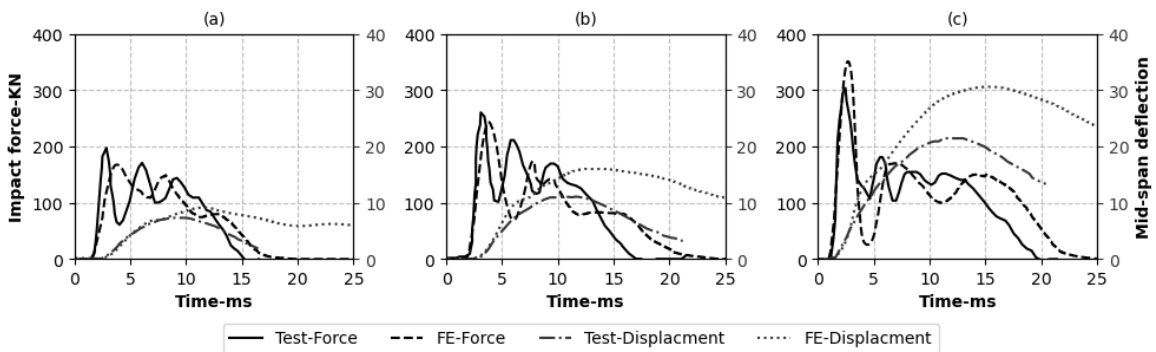


**Figure 3.6** Experimental and FE impact force and mid-span deflection time histories with different drop heights for beam series S2222 (a)  $H= 0.3\text{m}$ , (b)  $H= 0.6\text{m}$ , (c)  $H=1.2\text{m}$

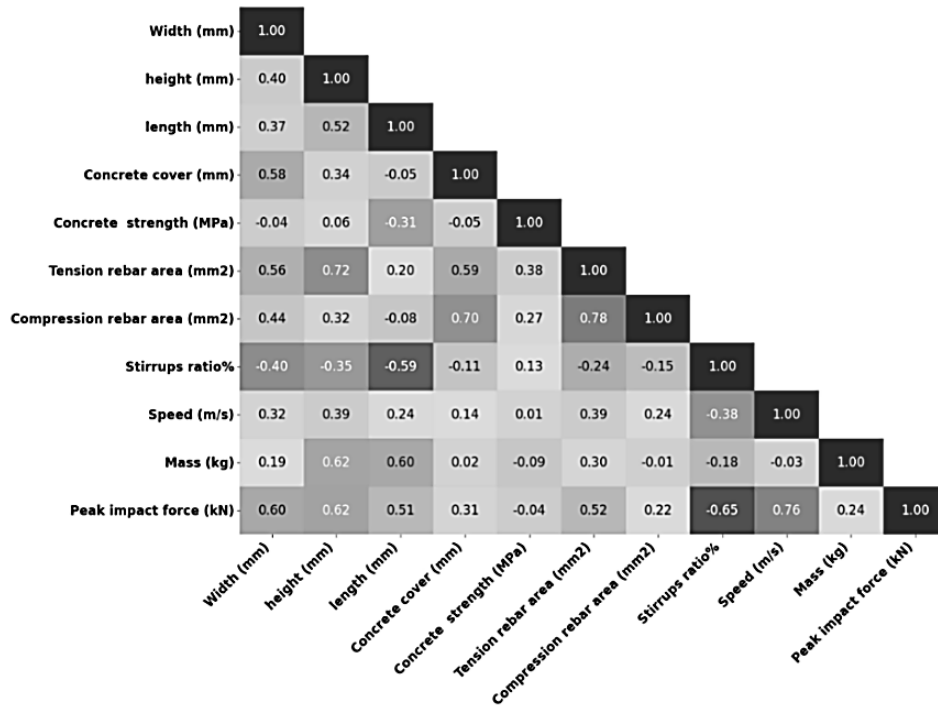
Many parameters that influence the beam impact performance including beam dimensions, concrete compressive strength, reinforcement yield strength, and impacting mass and speed, were investigated in Guo et al., Li et al., and Pham et al. [22-24]. To determine the most influential parameters on RC beams subjected to impact loads, machine learning (ML) algorithms were applied to a dataset of 140 reinforced concrete beams compiled by Zhao et al. [25].

Two ML algorithms were implemented to optimize the number of parameters. Predictions from different algorithms lead to confidence and a robust parameter selection. The Pearson correlation coefficient (Equation 3.1), and the importance ranking using the ExtraTree Classifier algorithm were implemented. The two algorithms are useful in understanding the correlation between a set of parameters and a target variable. In this case, the target variable was the peak impact force (Fig. 3.7). Based on the machine learning results, the impact speed, impact mass, beam mass, beam sectional area, reinforcement (RFT) ratio, and beam length positively correlate with the impact force (Fig. 3.7). Therefore, truck speed, truck mass, girder span, girder cross-section type, and shear reinforcement ratio were chosen for the parametric analysis. Where  $\text{cov}$  is the covariance, and  $\sigma_x$  and  $\sigma_y$  are the standard deviations of X and Y respectively.

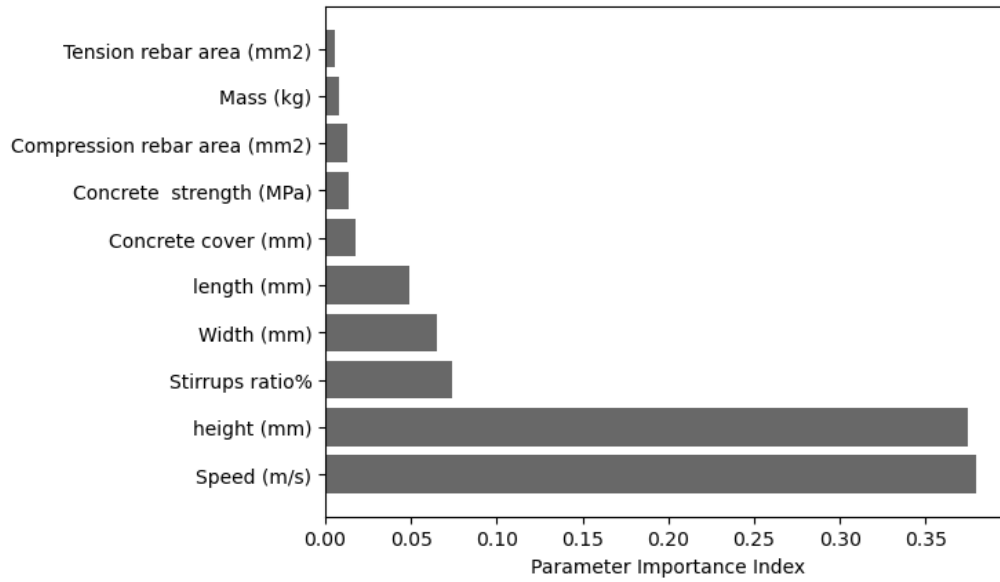
$$\rho = \frac{\text{cov}(x, y)}{\sigma_x \sigma_y} \quad (3.1)$$

To identify the most common feature of bridges in the U.S., another dataset containing 180,000 bridges with prestressed concrete girders was obtained from the National Bridge Inventory (NBI) and analyzed. Bridges were categorized in terms of span, skew angle, and bridge width (Fig. 3.8). Almost 50% of the bridges have a skew angle of zero to five degrees

(Fig. 3.8). Therefore, Oblique collisions were excluded from the study, where all the girders had zero skew angle to account for the most severe crash incidents. The selected span of girders (Fig. 11) was 15.24 m and 27.43 m based on the median of the existing bridges.



(a)



(b)

**Figure 3.7** ML algorithms (a) Heat map of the Pearson's Correlation coefficient, (b) Parameter Importance

A full bridge was considered in the parametric study to examine its behavior against the isolated girder. The bridge width was taken as the median of 13.50 m (Fig. 3.9). A total of nine girder-tractor-semi-trailer simulations were developed. The simulations involved collisions between the semi-trailer and isolated girders as well as on a full bridge for comparison. The full bridge and the isolated girders were designed according to the AASHTO LRFD. The isolated girder had a reinforced composite deck slab with a depth of 179 mm and an effective slab width of 2.28 m (Table 3.2). MoDot I - type 2, MoDot I - type 2, and MoDot NU 35 were chosen for the study (Fig. 3.9). The geometry of MoDot-type girders closely resembles AASHTO-type girders. The crash scenarios are described in (Table 3.3). The deck slab was constrained against translation and rotation from the collision opposite side to simulate a rigid condition, as shown in Figure 3.10.

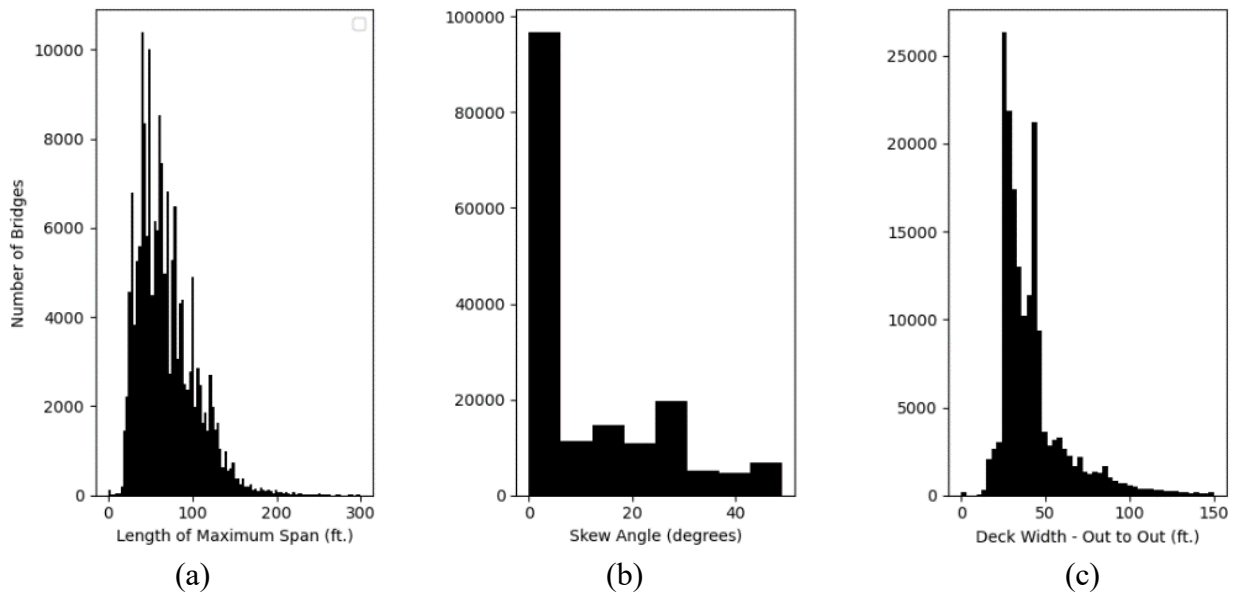


**Figure 3.8** (a) Number of bridges with the span, (b) skew angle, (c) deck width

**Table 3.2** Girder description and geometric summary

Description	MoDOT I-type 2	MoDOT I-type 6	MoDOT NU 35
Girder concrete strength (MPa )	41.40	41.40	41.4
Deck concrete strength (MPa)	34.45	None	None
Number of 0.5" strands	12	36	12
Deck depth (mm)	178	178	178
Deck effective width (mm)	7500	7500	7500
Strand type	Low relaxation 270 ksi	Low relaxation 270 ksi	Low relaxation 270 ksi
Mild steel tensile strength (MPa)	413	413	413

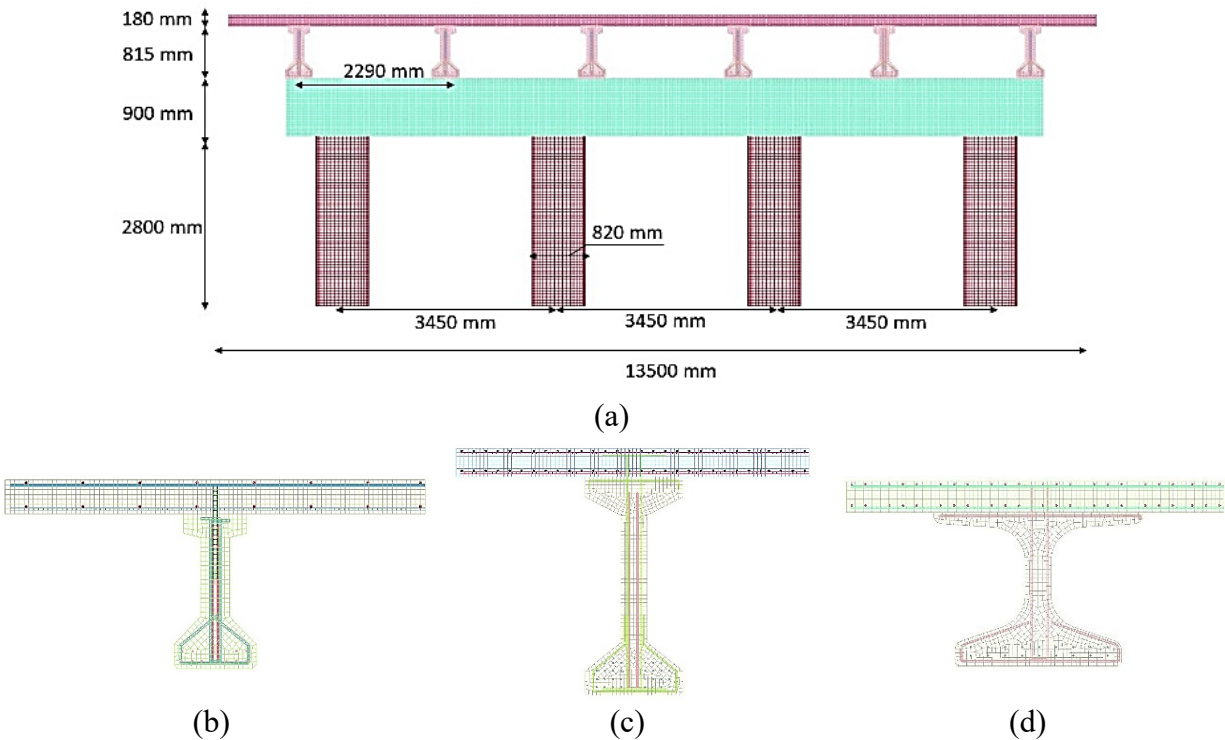
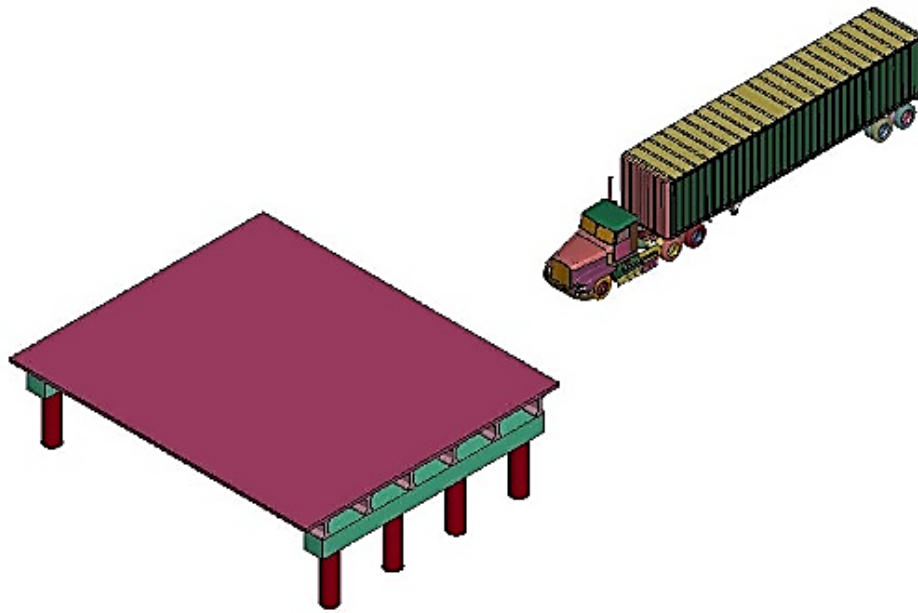


**Figure 3.9** FE models, (a) Full bridge of Modot type II; Isolated girders wot composite deck slab, (b) Modot type 2, (c) Modot type 6, (d) NU 35 girder.

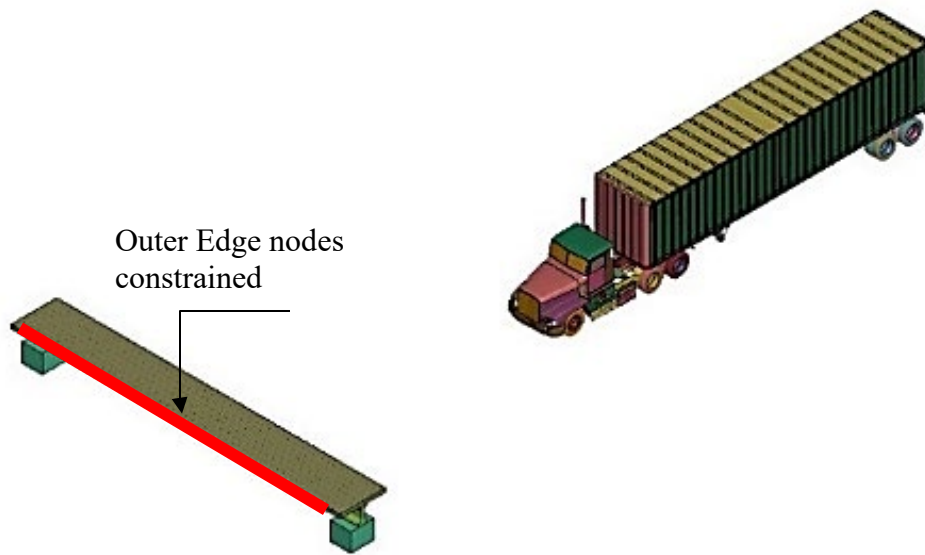
**Table 3.3** FE Study Parameters

Model number	Truck speed (Km/h)	Truck mass (Ton)	Span (m)	Bridge deck condition	Effect studied
01-M2-L15.24-S80-M24.9*	80	24.90	15.24	Full bridge	Reduced model
02-M2-L15.24-F80-M24.9*	80			Individual girder	
03-M2-L15.24-S48-M24.90*	48				Truck speed
04-M2-L15.24-S112-M24.90*	112				
05-M2-L15.24-S144-M24.9*	144				
06-M6-L15.24-S80-M24.90*	80		27.43		
07-M6-L27.43-S80-M27.43*	80				
08-NU35-L15.24-S80-M24.90*	80		15.24		
09-M2-L15.24-S80-M36.24*	80	36.24		Truck mass	

\*01-M2-L15.24-F80-M24.9: 01 is the incident number, M2 (girder type), L15.24 (girder overall length in meters), S80 for single girder and truck speed in km/h, F80 for full bridge and truck speed in km/h, M24.9 for truck mass in tons



(a)



(b)

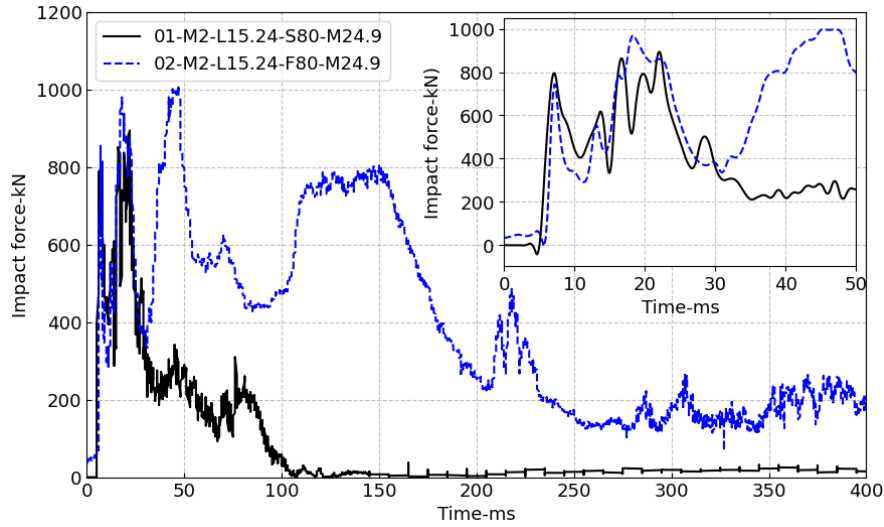
**Figure 3.10** FE 3D view (a) Full bridge, and (b) Isolated girder with composite deck (01-M2-L15.24-S80-M24.9)

## Chapter 4 Analysis of results, research report, and dissemination:

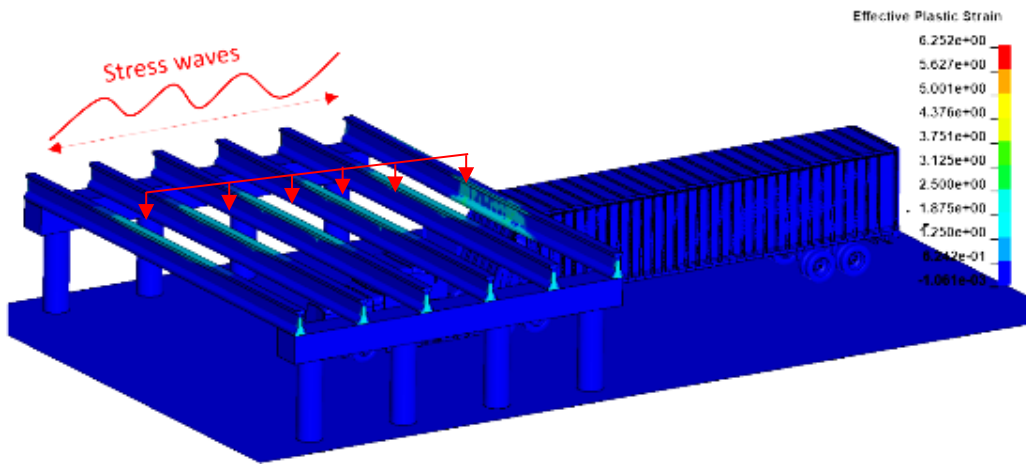
This section provides a comprehensive presentation of the results obtained from the finite element models described in Chapter 3. The validity of each model was established by comparing it to the available experimental data.

### 4.1 Effect of the isolated girder against the full bridge

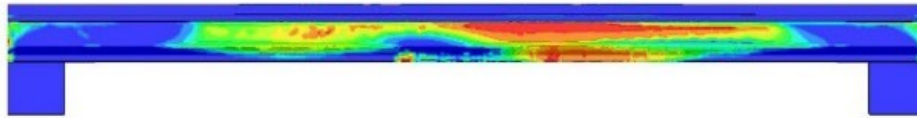
Figure 4.1a shows the impact force time history for the full bridge and isolated girder (01-M2-L15.24-S80-M24.9). Several impact force peaks were identified in the full bridge model due to the sequential collapse of the trailer roof against the girder. The full bridge peak impact force had an increase of 11.5% against the isolated girder. This can be attributed to the high lateral stiffness of the full bridge that prevents the composite deck from out-of-plane rotation. Also, the collision duration was four times longer than the isolated girder. This difference was attributed to the stress wave propagation through a medium as shown in Figure 4.1b and 4.1c). The longitudinal stress waves had to travel a longer distance from the impact region through the concrete medium before hitting the boundary and reflecting its source, thus prolonging the collision time as shown in Figure 4.1a. The damage is more substantial for the isolated girder (01-M2-L15.24-S80-M24.9) than the full bridge due to the increase of deck lateral stiffness and the absence of the remaining bridge girders' contribution. However, overall girder response and failure modes for both cases were relatively similar. Thus, a reduced model of an isolated girder composite deck was chosen for the remaining analyses to save the computation cost.



(a)



(b)



(c)

**Figure 4.1** FE results (a) full bridge and Isolated girder force time history, (b) full bridge damage, and (c) isolated girder damage (01-M2-L15.24-S80-M24.9)

## 4.2 Effect of Truck Speed

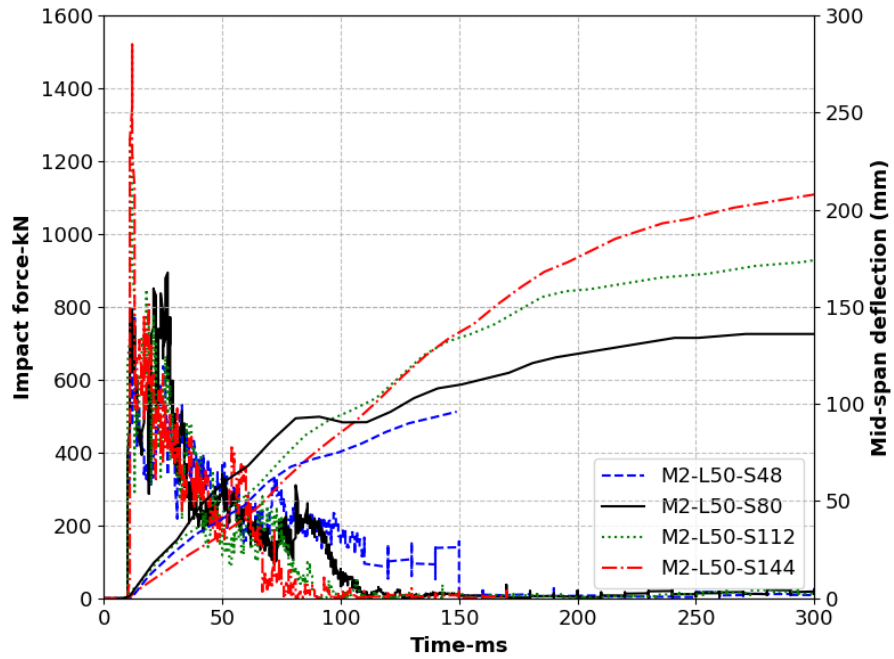
Figure 4.2 shows the impact time histories of a 24.9-ton semi-tractor trailer with a MoDot type 2 girder with different speeds. The plots were shifted by 10 milliseconds for clarity. The

peak impact force increased by 197% (from 769 kN to 1520 kN) with a 180% increase in the truck's speed from 48 to 144 km/h (Figure 4.2b). The impact force increase can be primarily credited to the impulse-momentum theorem (Equation 4.1-4.2). The impulsive force resulting from the impact of the truck is related to the change in momentum (Equation 4.1). The displacement time histories depicted that the maximum girder dynamic response in terms of mid-span displacement increased by 116%, from 98 mm to 212 mm, when increasing the impact speed from 48 to 144 km/h, respectively. Figure 4.2 shows the collision time decreases slowly as impact speed increases, thereby increasing the impact force. The reduction in collision duration due to impact speed can be attributed to the contact mechanics, as when the impacting body collides at higher speeds it stays in contact for less time with the impacted object before rebounding. Diagonal shear cracking can be observed along the girder for all speeds which has been reported in several past studies (Figure 4.3). Shear failures were more visible and pronounced as the speed of the impact increased from 48 to 144 km/h.

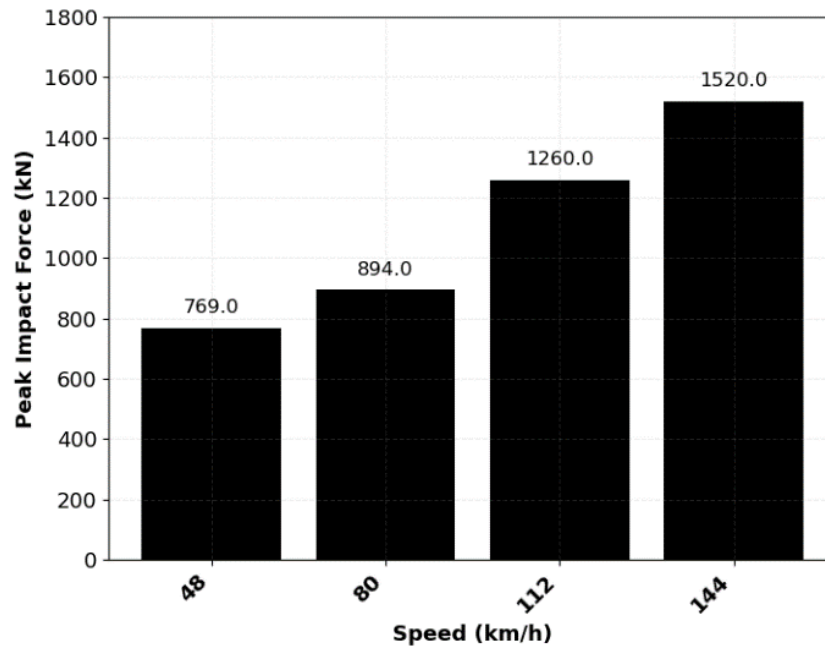
$$\int_{t_1}^{t_2} F dt = \Delta p \quad (4.1)$$

$$I = \Delta p \quad (4.2)$$

Where I is the impulse,  $\Delta p$  is the change of linear momentum of the dynamic system after and before the impact, and t is the impact duration.



(a)



(b)

**Figure 4.2** (a) Impact force and displacement time histories, (b) Peak impact force with speed

### 4.3 Effect of Truck Mass

Figure 4.4 illustrates the impact force-time history of two truck masses, 24.9 tons and 36.3 tons, both traveling at a constant speed of 80 km/h. The 145% increase in truck mass resulted in a moderate 12% rise in peak impact force, from 900 kN to 1010 kN, occurring between collision times of 7 to 22 ms. Additionally, in the previous section, a 140% increase in impact speed from 80 km/h to 112 km/h led to a 40% surge in peak impact force, from 894 kN to 1260 kN (Fig. 4.4). These finite element (FE) findings were well-aligned with the Pearson correlation coefficient derived from machine learning for reinforced concrete beams under impact loads, revealing correlation factors of 0.24 and 0.76 for impact mass and impact speed, respectively, concerning the peak impact force. Notably, the correlation coefficient increases of 3.1% from 0.24 to 0.76 corresponds to a 3.3% increase in the peak impact force resulting from the impact speed (40%) and mass (12%) parameters. Additionally, these findings demonstrate the fidelity of the FE model in simulating the impact behavior of the BPCG.

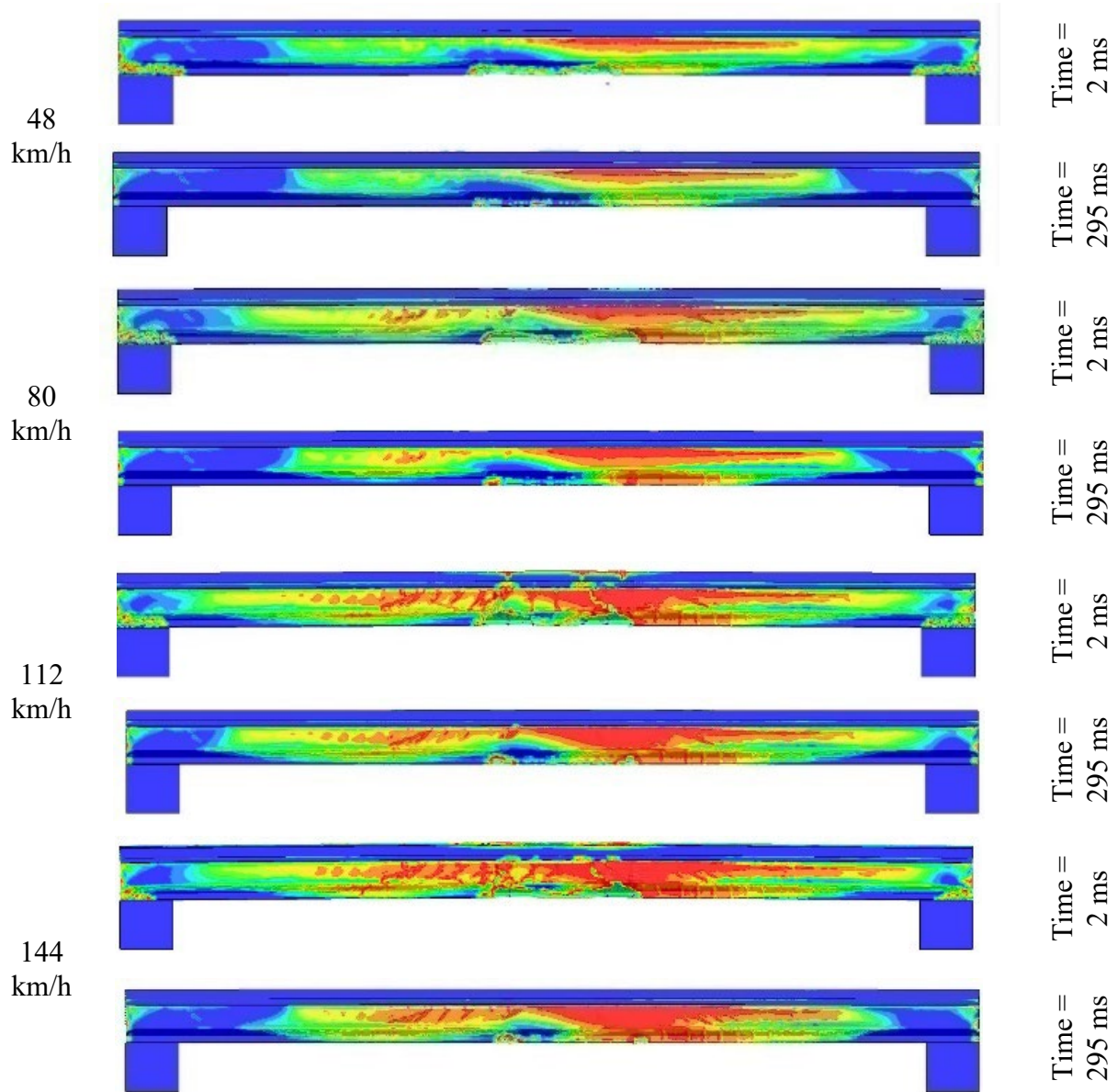
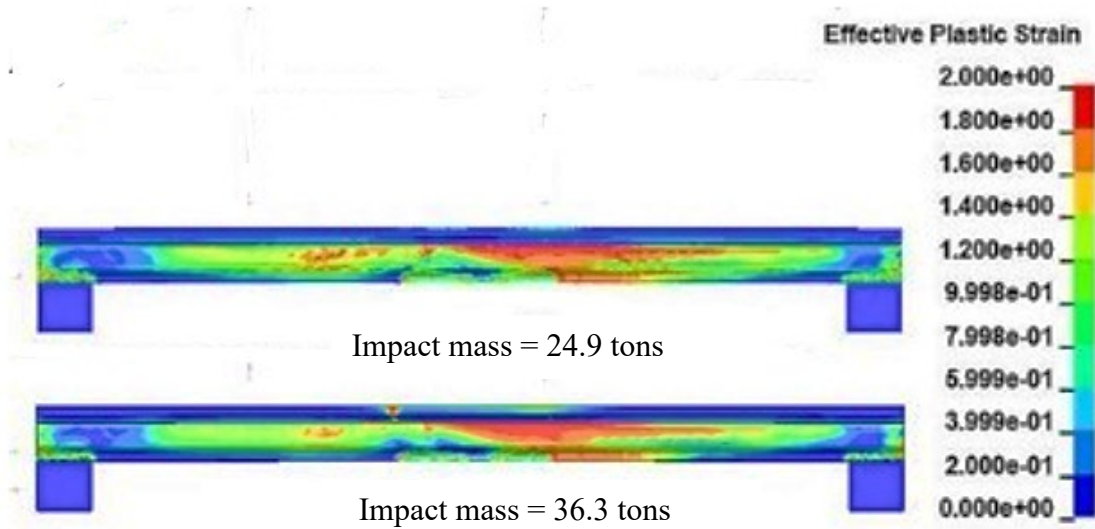
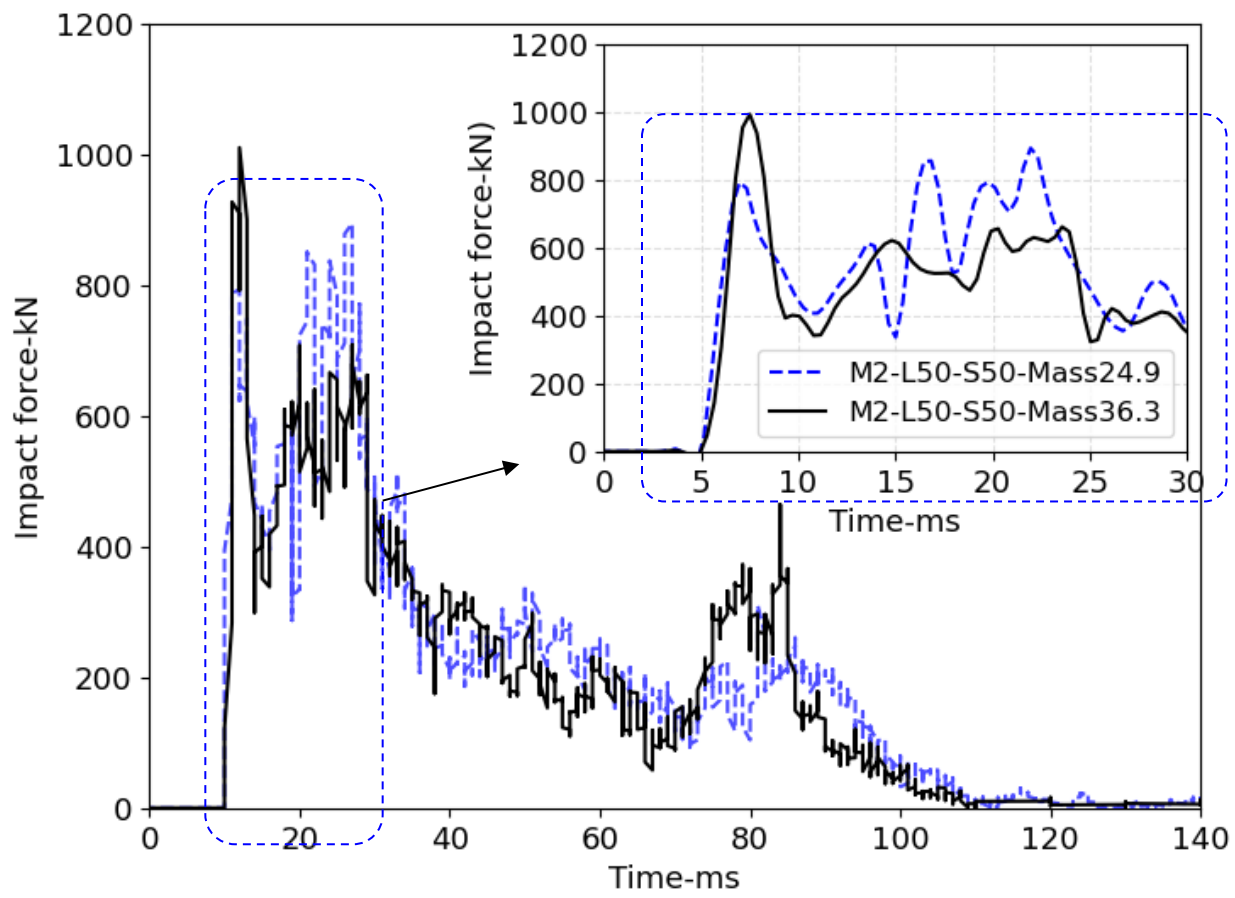


**Figure 4.3** The contour of plastic strain Damage modes (a) at the first impact, (b) at maximum displacement ( $t=30$  ms)



(a)



(b)

**Figure 4.4** (a) Impact force-displacement time histories and damage modes for truck mass 24.9 and 36.3 tons (b) Impact time histories details

## Chapter 5 Conclusions

Comprehensive numerical analyses were undertaken to validate a finite element model for prestressed concrete girders under both static and impact loading conditions. The developed finite element models were effectively implemented, and an in-depth parametric study was executed. Several methods for modeling prestressed concrete have been investigated using the LS-DYNA software, including stress initialization, axial beam force, and temperature-induced shrinkage. The effect of using dynamic relaxation in modeling prestressed concrete was also introduced. The selection of an appropriate concrete constitutive material model was thoroughly debated to ensure the model appropriately represented the response of prestressed girder bridges under impact loads. Four material models were investigated and evaluated: CSCM, CDPM, KCC, and Winfirth. The selection of study parameters was based on machine learning and data analysis of the available literature. Following that, a series of validation steps were carried out to ensure the FE model accurately reflected the behavior of a real full-scale bridge.

Based on the results of the study, the following conclusions were drawn.

1. The finite element modeling of an entire bridge structure can be substantially simplified by utilizing an isolated girder configuration with an integrated composite deck slab, necessitating careful modeling and complete constraint from the impact-facing side.
2. The increase of tractor semi-trailer speed by 140%, significantly increased the peak impact force by 64%.
3. Collision timing depends upon dynamic properties intrinsic to the structure, encompassing stiffness and girder type, as well as the loading conditions defined by impact velocity.

4. An increase in tractor-semi-trailer mass by 145% resulted in a slight augmentation of peak impact forces by 12%.
5. The application of dynamic relaxation in explicit analysis models is essential for reducing stress value oscillations. These dynamic effects could be minimized by employing dynamic relaxation with an appropriate convergence tolerance, resulting in more stable and steady-state conditions.
6. The impactor's speed has a significant effect on the impact force experienced by the girder. Higher speeds correspond to greater kinetic energy, resulting in a larger amount of impact energy transferred to the girder. Therefore, the impact force tends to be greater for faster impactors.

## References

1. Agrawal, Anil K., Sherif El-Tawil, Ran Cao, Xiaochen Xu, Xiaoxuan Chen, and Waider Wong. *A performance-based approach for loading definition of heavy vehicle impact events*. No. FHWA-HIF-18-062. United States. Federal Highway Administration. Office of Research, Development, and Technology, 2018.
2. Abdelkarim, Omar I., and Mohamed A. ElGawady. "Performance of hollow-core FRP–concrete–steel bridge columns subjected to vehicle collision." *Engineering Structures* 123 (2016): 517-531.
3. Oppong, K., Saini, D., & Shafei, B. (2021a). Characterization of impact-induced forces and damage to bridge superstructures due to over-height collision. *Engineering Structures*, 236, 112014. <https://doi.org/10.1016/j.engstruct.2021.112014>
4. Oppong, K., Saini, D., & Shafei, B. (2021b). Ultrahigh-performance concrete for Improving Impact Resistance of Bridge Superstructures to Overheight Collision. *Journal of Bridge Engineering*, 26(9), 04021060. [https://doi.org/10.1061/\(asce\)be.1943-5592.0001736](https://doi.org/10.1061/(asce)be.1943-5592.0001736)
5. Fu, Y., Yu, X., Dong, X., Zhou, F., Ning, J., Li, P., & Zheng, Y. (2020). Investigating the failure behaviors of RC beams without stirrups under impact loading. *International Journal of Impact Engineering*, 137, 103432. <https://doi.org/10.1016/j.ijimpeng.2019.103432>
6. Kishi, N., Mikami, H., Matsuoka, K. G., & Ando, T. (2002). Impact behavior of shear-failure-type RC beams without shear rebar. *International Journal of Impact Engineering*, 27(9), 955–968. [https://doi.org/10.1016/S0734-743X\(01\)00149-X](https://doi.org/10.1016/S0734-743X(01)00149-X)
7. Kishi, N., Ohno, T., Konno, H., & Bhatti, A. Q. (2006). Dynamic response analysis for a large-scale RC girder under a falling-weight impact loading. *Solid Mechanics and Its Applications*, 140, 99–109. [https://doi.org/10.1007/1-4020-4891-2\\_8](https://doi.org/10.1007/1-4020-4891-2_8)
8. Kishi, N. (2019). Numerical simulation of reinforced concrete structures under impact loading. *Materialwissenschaft Und Werkstofftechnik*, 50(5), 599–610. <https://doi.org/10.1002/mawe.201800181>
9. Kelly, J., *The effects of impact loading on prestressed concrete beams*. 2011, Ph. D. thesis, Heriot-Watt Univ., Edinburgh, Scotland.
10. Jing, Y., Ma, Z. J., & Clarke, D. B. (2016). Full-scale lateral impact testing of prestressed concrete girder. *Structural Concrete*, 17(6), 947–958. <https://doi.org/10.1002/suco.201500224>
11. Thilakarathna, H. M. I., D. P. Thambiratnam, Manicka Dhanasekar, and Nimal Perera. "Numerical simulation of axially loaded concrete columns under transverse impact and

- vulnerability assessment." *International Journal of Impact Engineering* 37, no. 11 (2010): 1100-1112.
12. Zhang, Jingfeng, Xiaozhen Li, Yuan Jing, and Wanshui Han. "Bridge structure dynamic analysis under vessel impact loading considering soil-pile interaction and linear soil stiffness approximation." *Advances in Civil Engineering* 2019 (2019).
  13. Qiao, Pizhong, Mijia Yang, Ayman Mosallam, and Gangbing Song. *An over-height collision protection system of sandwich polymer composites integrated with remote monitoring for concrete bridge girders*. No. FHWA/OH-2008/6. University of Akron. Dept. of Civil Engineering, 2008.
  14. Miele, C. R., Plaxico, C., Stephens, D., & Simunovic, S. (2010). U26: Enhanced Finite Element Analysis Crash Model of Tractor-Trailers (Phase C). Phase C, 276p.
  15. O'toole, B., K. Karpanan, and M. Fegghi. *Experimental and finite element analysis of preloaded bolted joints under impact loading*. in *47th AIAA/ASME/ASCE/AHS/ASC Structures, Structural Dynamics, and Materials Conference 14th AIAA/ASME/AHS Adaptive Structures Conference 7th*. 2006.
  16. Hadjioannou, M., D. Stevens, and M. Barsotti. *Development and validation of bolted connection modeling in LS-DYNA® for large vehicle models*. in *14th International LS-DYNA Users Conference*. 2016.
  17. Thai, Huu-Tai, Vo, Thuc, Nguyen, Trung-Kien and Pham, Cao Hung (2017) Explicit simulation of bolted endplate composite beam-to-CFST column connections. *Thin-Walled Structures*, 119. pp. 749-759. ISSN 0263-8231
  18. Wu Y, Crawford JE. Numerical Modeling of Concrete Using a Partially Associative Plasticity Model. *J Eng Mech*. 2015;141(12):04015051.
  19. Chehab, A. I., Eamon, C. D., Parra-Montesinos, G. J., & Dam, T. X. (2018). Shear testing and modeling of AASHTO type II prestressed concrete bridge girders. *ACI Structural Journal*, 115(3), 801–812. <https://doi.org/10.14359/51701917>
  20. Olsen, S. A. (1992). Reusability and Impact Damage Repair of Twenty-Year-Old AASHTO Type III girders.
  21. Ludovico. (2005). Repair of Bridge Girders with Composites: Experimental and Analytical Validation. *ACI Structural Journal*, 102(5). <https://doi.org/10.14359/14659>
  22. Guo, J., Cai, J., & Chen, W. (2017). Inertial Effect on RC Beam Subjected to Impact Loads. *International Journal of Structural Stability and Dynamics*, 17(4), 1–23. <https://doi.org/10.1142/S0219455417500535>

23. Li, H., Chen, W., & Hao, H. (2020). Factors influencing impact force profile and measurement accuracy in drop weight impact tests. *International Journal of Impact Engineering*, 145(February 2021). <https://doi.org/10.1016/j.ijimpeng.2020.103688>
24. Pham, T. M., & Hao, H. (2017). Effect of the plastic hinge and boundary conditions on the impact behavior of reinforced concrete beams. *International Journal of Impact Engineering*, 102, 74–85. <https://doi.org/10.1016/j.ijimpeng.2016.12.005>
25. Zhao, W., Qian, J., Jia, P., 2019. Peak Response Prediction for RC Beams under Impact Loading. *Shock Vib.* 2019. <https://doi.org/10.1155/2019/6813693>